Sound Propagation in a Bose-Fermi Mixture: From Weak to Strong Interactions

Krutik Patel, Geyue Cai, Henry Ando, and Cheng Chin

Sound propagation in a Bose-Fermi mixture: from weak to strong interactions

Krutik Patel, Geyue Cai, Henry Ando, and Cheng Chin

The James Franck Institute, Enrico Fermi Institute, and Department of Physics,
The University of Chicago, Chicago, IL 60637, USA

Particle-like excitations, or quasi-particles, emerging from interacting fermionic and bosonic quantum fields underlie many intriguing quantum phenomena in high energy and condensed matter systems. Computation of the properties of these excitations is frequently intractable in the strong interaction regime. Quantum degenerate Bose-Fermi mixtures offer promising prospects to elucidate the physics of such quasi-particles. In this work, we investigate phonon propagation in an atomic Bose-Einstein condensate immersed in a degenerate Fermi gas with interspecies scattering length a_{BF} tuned by a Feshbach resonance. We observe sound mode softening with moderate attractive interactions. For even greater attraction, surprisingly, stable sound propagation re-emerges and persists across the resonance. The stability of phonons with resonant interactions opens up opportunities to investigate novel Bose-Fermi liquids and fermionic pairing in the strong interaction regime.

Interactions between excitations of bosonic and fermionic quantum fields play an important role in understanding fundamental processes in high energy and condensed matter physics. In quantum electrodynamics, for example, the coupling between the photon and virtual electron-positron pairs polarizes the vacuum, which contributes to Lamb shifts [1] and the anomalous magnetic moments of the electron and the muon [2]. In condensed matter, interactions between phonons and electrons are central to Cooper pairing in conventional superconductors [3], as well as charge ordering and superconductivity in strongly correlated materials [4, 5].

Ultracold mixtures of atomic Bose and Fermi gases offer a complementary experimental platform for elucidating these quantum phenomena. Cold atoms are exceptionally flexible, allowing for the control of interactions between the atomic species using Feshbach resonances [6]. These capabilities have been used to study phase transitions in lattices [7–9], polarons [10, 11], and superfluid mixtures [12, 13]. Many exciting theoretical predictions for quantum simulation remain to be tested, e.g. Refs. [14–16].

In this work, we investigate sound propagation in a quantum degenerate Bose-Fermi mixture from the weak to the strong interaction regime. We optically excite density waves in the gases and measure their velocities and damping rates from *in situ* images of the Bose-Einstein condensate (BEC). We see significant changes in the speed of sound for interspecies attraction and negligible shifts for repulsion. This asymmetry indicates strong deviation from the perturbation prediction. Intriguingly, we find stable propagation of sound waves in mixtures with resonant interspecies interactions. This observation offers promising prospects to explore new quantum phases of Bose-Fermi mixtures in the strong interaction regime.

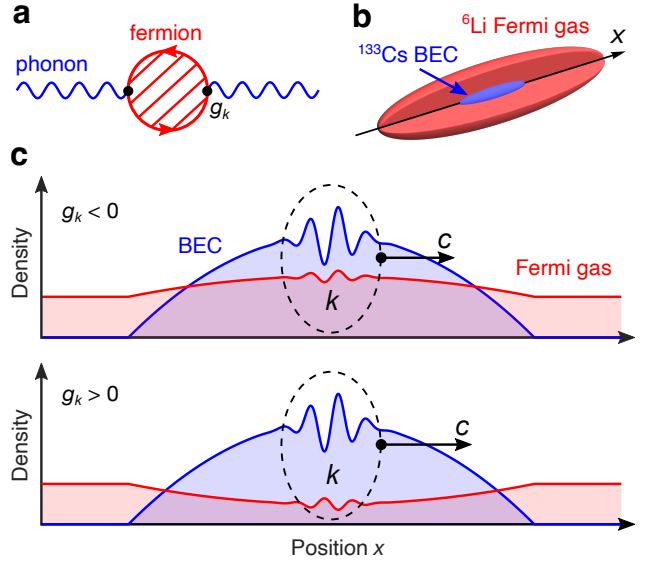The Hamiltonian for the phonons coupled to a single-component Fermi gas is given by [17, 18]

FIG. 1. Bosonic quasi-particles (phonons) coupled to a fermionic quantum field. (a) Diagrammatic representation of phonons (blue) coupled to excitations of a fermionic field (red). The lowest order diagram contains a single loop and is second order in the phonon-fermion coupling g_k. Higher order corrections are indicated by the hatched area. (b) In our experiment, a cigar-shaped Bose-Einstein condensate (BEC) of cesium-133 is immersed in a much larger degenerate Fermi gas of lithium-6. (c) As a phonon with momentum k (black dashed ellipse) propagates, the coupling results in the density modulation of both species and the modification of the sound speed c.

$$H = \sum_k \epsilon_k^{\mathrm{F}} c_k^\dagger c_k + \sum_k \hbar\omega_k \alpha_k^\dagger \alpha_k + \sum_{k,q} g_k(\alpha_k + \alpha_{-k}^\dagger)c_q^\dagger c_{q-k},$$

(1)

where ϵ_k^{F} is the dispersion of the fermions, $\hbar$ is the reduced Planck's constant, ω_k is the phonon dispersion, g_k is the phonon-fermion coupling constant, c_k and α_k refer to fermion and phonon annihilation operators respec-
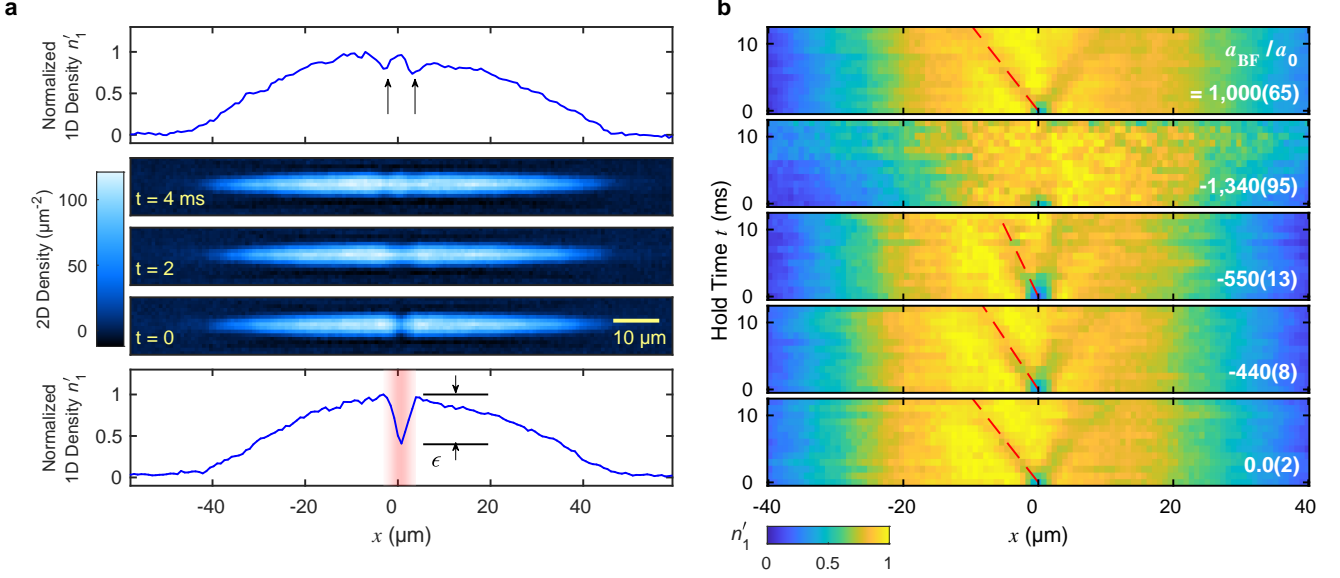
FIG. 2. Excitation and *in situ* imaging of density waves. (a) A local density depletion ϵ is created in the center of the cesium BEC by a projected laser beam (bottom panel, red shaded area). The optical potential is abruptly switched off at $t = 0$ and the density dip splits into density waves propagating in opposite directions (top panel, black arrows). Average column densities are shown for three values of the hold time $t = 0, 2, 4$ ms along with sample normalized one-dimensional (1D) densities n'_1 for $t = 0$ ms and $t = 4$ ms. Data is shown for the Cs-Li Bose-Fermi mixture with interspecies scattering length $a_{BF} = -335\,a_0$. (b) Normalized 1D densities n'_1 show density wave dynamics for mixtures prepared at various interspecies scattering lengths. Red dashed lines are guides to the eye.

tively, and k and q are momenta (see Fig. 1a). In our degenerate Bose-Fermi mixture, the kinetic energy of a bare fermion is $\epsilon_k^F = \hbar^2 k^2 / 2m_F$, where m_F is the fermion mass. The bare phonons are low energy excitations of the BEC with the Bogoliubov dispersion [19] $\omega_k \approx c_0 k$, where the sound velocity $c_0 = \sqrt{g_{BB} n_B / m_B}$ is determined by the boson-boson coupling constant g_{BB}, condensate density n_B, and boson mass m_B. The phonon-fermion coupling constant is $g_k = g_{BF} \sqrt{n_B \hbar^2 k^2 / 2m_B \omega_k}$ [18, 20], where $g_{BF} = 2\pi\hbar^2 a_{BF}/m_r$ is the interspecies coupling constant, a_{BF} is the interspecies scattering length and m_r is the reduced mass of the two unlike atoms. The phonon-fermion coupling g_k can thus be tuned by controlling a_{BF} using an interspecies Feshbach resonance (see Fig. 1c).

Perturbation theory shows that the velocity of phonons is reduced when the BEC interacts weakly with the Fermi gas. This can be understood as a result of a fermion-mediated interaction between bosons analogous to the Ruderman-Kittel-Kasuya-Yosida mechanism [21, 22]. The mediated interaction has been observed in cold atom experiments [23, 24]. To leading order in g_{BF}, the sound velocity is predicted to be [25]

$$ c = c_0 \sqrt{1 - \frac{3}{2}\frac{g_{BF}^2}{g_{BB}}\frac{n_{F0}}{E_{F0}}}, \qquad (2) $$

where n_{F0} and E_{F0} are the density and Fermi energy of the Fermi gas in the absence of the condensate. This

correction is quadratic in the coupling strength g_{BF}, and corresponds to the one-loop diagram shown in Fig 1a. The sound speed is expected to be reduced regardless of the sign of the interspecies coupling strength g_{BF}. The perturbation result is valid in the weak coupling regime $|g_{BF}n_B| \ll E_{F0}$.

At stronger interactions, the density profile of each species can be significantly modified by the other species. This effect can be captured in a mean-field model. Under the Thomas-Fermi approximation for both species, the local mean-field chemical potential of the bosons depends on the fermion density as [20]

$$ \mu_{TF} = g_{BB}n_B + g_{BF}n_{F0}\left(1 - \frac{g_{BF}n_B}{E_{F0}}\right)^{3/2}, \qquad (3) $$

where the second term is set to zero when the mean-field interaction energy exceeds the Fermi energy, $g_{BF}n_B > E_{F0}$. In our system, it is a good approximation that the light fermions (Li) follow the heavy bosons (Cs) adiabatically. This permits the evaluation of the mean-field sound speed $c = \sqrt{n_B/m_B\kappa}$ in terms of the effective compressibillity $\kappa = \partial n_B/\partial\mu_{TF}$ as

$$ c = c_0 \sqrt{1 - \frac{3}{2}\frac{g_{BF}^2}{g_{BB}}\frac{n_{F0}}{E_{F0}}\sqrt{1 - \frac{g_{BF}n_B}{E_{F0}}}}. \qquad (4) $$

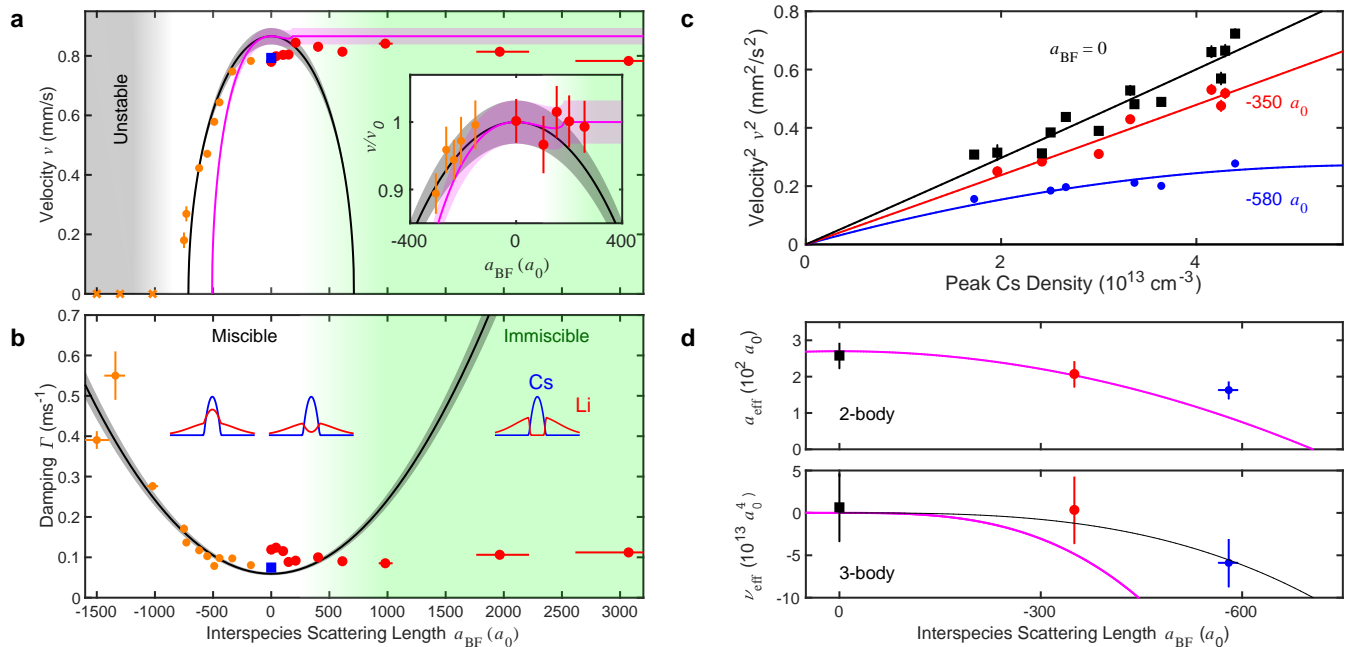Compared to Eq. (2), the additional factor in Eq. (4)

FIG. 3. Sound speeds and damping rates at different interspecies scattering lengths and boson densities. (a) Orange data points indicate samples prepared on the attractive side of the Feshbach resonance $a_{BF} < 0$. Red data points are prepared on the repulsive side with $a_{BF} > 0$. Measurement for a bare BEC without femions is shown as the blue square. The crosses indicate samples with no stable sound propagation. Inset shows the ratio of density wave velocities for samples prepared with and without the fermions. The ratios are obtained from the separation of density waves after 8 ms hold time. Calculations from perturbation (black line) and mean-field (magenta line) theory are shown for comparison. The green shaded area represents the phase separation region. The grey area indicates the region where no stable sound propagation is observed. (b) Damping rates of the density waves are compared with the perturbative prediction (black line) evaluated for momentum $k = 2\pi/(4\mu m)$ [20]. Insets: Cartoon representation of the Cs (blue) and Li (red) density profiles in different regimes. (c) Density wave velocities for BECs prepared without the Fermi gas (black squares) and with the Fermi gas at $a_{BF} = -350\,a_0$ (red circles) and $a_{BF} = -580\,a_0$ (blue circles). Lines are fits of the data to a model with both two- and three-body effective interactions between bosons (see text). (d) Colored circles are the effective scattering lengths and hypervolumes extracted from panel (c). The magenta lines are the mean-field predictions and the black line is a cubic fit to the data. The vertical error bars on the data in (a)-(c) are standard errors calculated from fits to averaged experimental density profiles. The horizontal error bars on the data in panels (a), (b), and (d) represent the 1-σ uncertainty of the scattering length [20]. The shaded regions around the theory calculations in panels (a) and (b) indicate the ranges of the predictions [20]. The error bars in panel (d) are standard errors calculated from fits to the data in panel (c).

captures the density changes in the mixture caused by interspecies interactions.

Our experiments begin with mixtures of a pure BEC of 30,000 ^{133}Cs atoms and a degenerate Fermi gas of 8,000 ^{6}Li atoms. Both species are spin polarized into their lowest hyperfine ground states [20, 26]. For Cs, this state is adiabatically connected to $|F = 3, m_F = 3\rangle$ and for Li it is connected to $|F = 1/2, m_F = 1/2\rangle$ at low magnetic fields, where F is the total angular momentum quantum number and m_F is the magnetic quantum number. The mixture is trapped in a single beam optical dipole trap at wavelength 1064 nm with trap frequencies $\omega_{Cs} = 2\pi \times (6.53, 100, 140)$ Hz and $\omega_{Li} = 2\pi \times (36, 330, 330)$ Hz in the axial and two transverse directions. The bosons and fermions have a temperature of about 30 nK and chemical potentials of about $k_B \times 30$ nK and $k_B \times 300$ nK respectively, where k_B is the Boltzmann constant. In the

dipole trap, the BEC is fully immersed in the degenerate Fermi gas (see Fig. 1b). We tune the interspecies scattering length near a narrow Feshbach resonance at magnetic field 892.65 G [20, 27, 28]. Across the resonance, the boson-boson interactions are moderately repulsive with a nearly constant scattering length $a_{BB} = 270\,a_0$ [29], where a_0 is the Bohr radius. At these temperatures, the interactions between the single component Li atoms are negligible. In our experiment, the mixture is prepared in the weak coupling regime, where the interspecies scattering length is $|a_{BF}| < 200a_0$.

To study sound propagation in our system, we optically excite density waves in the mixture [30–32]. We introduce a narrow repulsive potential barrier of width $\delta = 4$ μm by projecting blue-detuned light onto the center of the BEC, resulting in a density dip. We then switch the magnetic field to the target scattering length. After
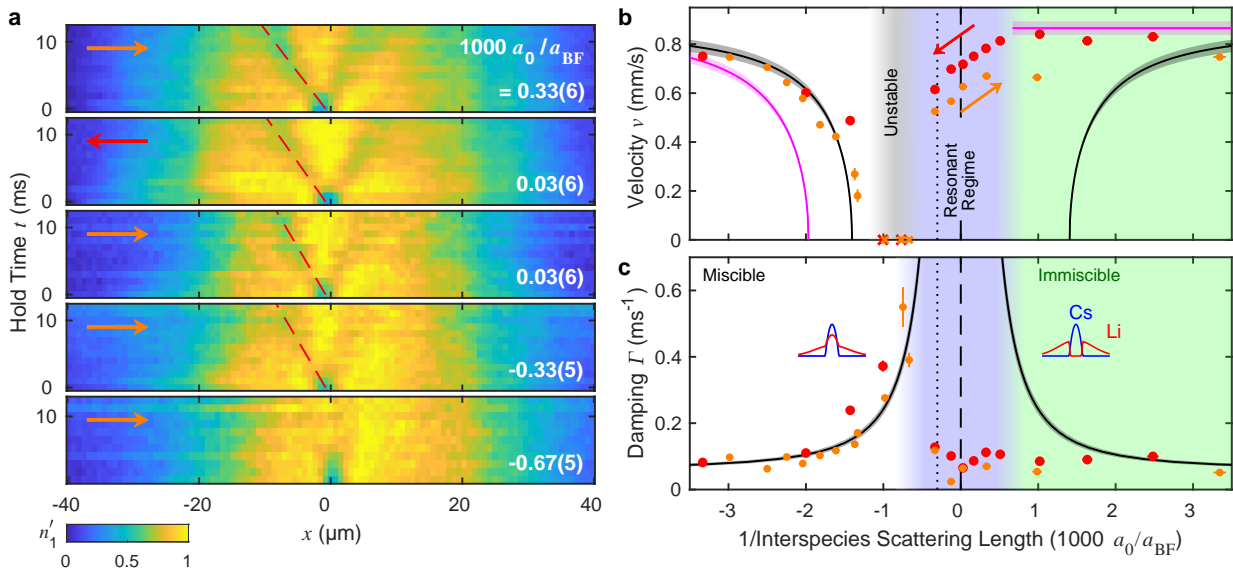
FIG. 4. Sound propagation across the Feshbach resonance. (a) Normalized 1D densities illustrating the revival of sound propagation at strong interactions based on the same experimental procedure as in Figs. 2 and 3. The arrows on each data set indicate whether the system is ramped towards the resonance starting from the attractive side (orange arrow) or repulsive side (red arrow). Red dashed lines are guides to the eye. (b) Density wave velocity of the Li-Cs mixture across the Feshbach resonance. Data taken from samples prepared on the attractive (repulsive) side are orange (red) in color. The arrows indicate the direction of the scattering length ramp. The blue and green regions indicate the resonant and phase separation regimes respectively. (c) Damping from the same data set. The black and magenta lines are the same perturbation and mean field predictions as shown in Fig. 3. The vertical error bars in panels (b) and (c) are standard errors from fits to averaged density profiles. The shaded regions around the theory curves in panels (b) and (c) indicate the ranges of the predictions [20]. The vertical dashed line shows the position of the Feshbach resonance. The vertical dotted line shows the position of the Efimov resonance reported in Ref. [28].

5 ms, when the magnetic field stabilizes, we turn off the optical barrier and record the dynamics of the density waves after various hold times t [20]. We observe that the initial density depletion splits into two density waves that counter-propagate at the same speed along the axial direction (see Fig. 2a). From the images, we extract the velocity v and damping rate Γ of the density waves [20]. We repeat the experiment at different interspecies interaction strengths (see Fig. 2b).

The density wave velocity v in a bare elongated condensate is given by the sound speed c_0 through [20, 33]

$$v \approx \frac{c_0}{\sqrt{2}}\sqrt{1 - \frac{\epsilon}{2}},\qquad(5)$$

where ϵ is the initial density depletion due to the potential barrier (see Fig. 2a) and c_0 is the sound speed at the center of the BEC.

In the presence of fermions, we measure the dependence of the density wave velocity on the initial density depletion ϵ and find agreement with Eq. (5) [20]. Thus, we adopt Eq. (5) to link the density wave velocity to the sound speed. In the following experiments, the initial density depletion is set to $\epsilon = 0.5$.

We summarize the measured density wave velocities and damping rates in Figs. 3a and 3b. As we increase the interspecies attraction from zero, the density waves propagate slower and decay faster. The enhanced damping of the density waves is consistent with the perturbation calculation for a zero-temperature Bose-Fermi mixture [17, 20]. When the scattering length exceeds the critical value of $a_c = -790(10)\,a_0$ [20], we no longer observe stable propagation of sound. Our finding is consistent with the sound mode softening in the Bose-Fermi mixture with increasing attraction. Our measured critical value shows clear deviations from the perturbation prediction $-710\,a_0$ and the mean field prediction $-510\,a_0$ for the collapse of the mixture [34].

For repulsive interspecies interactions, on the other hand, the density waves propagate with low damping and no significant change in velocity over the range we explore (see Figs. 3a and 3b). This is in stark contrast to our observations for attraction. The clear asymmetry with respect to the sign of the interaction goes beyond the perturbation prediction, see Eq. (2), which only depends on the square of the scattering length a_{BF}^2.

The asymmetry can be understood from the mean-field picture. For attractive interactions, fermions are pulled

into the BEC, and the higher fermion density further reduces the sound velocity. On the other hand, for repulsion, fermions are expelled from the BEC, reducing their effect on the sound propagation. For strong enough repulsion, the bosons and fermions are expected to phase separate [34–36]. The observed nearly constant sound velocity for strong repulsion is consistent with the picture that most fermions are expelled from the condensate. For our system, the mean field model predicts phase separation near the scattering length $a_{BF} \approx 180\,a_0$.

This asymmetry comes fundamentally from effective few-body interactions in the BEC that go beyond the perturbation calculation [37, 38]. The change of the density overlap, described in the mean-field picture, is a consequence of the few-body interactions. The effective boson-boson-boson three-body interaction strength can be experimentally characterized by writing the chemical potential in orders of the boson density

$$\mu = g_2 n_B + g_3 n_B^2 + ..., \qquad (6)$$

where $g_2 = 4\pi\hbar^2 a_{eff}/m_B$ and $g_3 \equiv \hbar^2\nu_{eff}/m_B$ are effective two- and three-body coupling constants between bosons, a_{eff} is the effective scattering length, and ν_{eff} is the effective scattering hypervolume. From the effective chemical potential μ we obtain the sound speed as $c \approx \sqrt{(g_2 n_B + 2 g_3 n_B^2)/m_B}$.

To determine the effective two- and three-body interaction strengths, we measure the density wave velocity at various boson densities and scattering lengths. The results are shown in Fig. 3c. From fits to the density wave velocities and Eqs. (5) and (6), we extract the effective scattering length a_{eff} and effective scattering hypervolume ν_{eff} (see Fig. 3d).

As the interspecies attraction increases, we observe a reduction of the effective scattering length, consistent with Ref. [23], and an emerging scattering hypervolume. Mean-field theory predicts $\nu_{eff} = \lambda a_{BF}^3$ with $\lambda \approx 159 k_F^{-1}$ set by the Fermi momentum and mass ratio [20]. Fitting the data, we determine $\lambda = 35(8) k_F^{-1}$, see Fig. 3d. This value shows clear deviation from the mean field prediction. Notably, the three-body interaction $g_3 n_B^2 \propto a_{BF}^3$ is the leading order process that breaks the symmetry between positive and negative scattering length.

By ramping our magnetic field across the Feshbach resonance, we explore the sound propagation in the strong interaction regime, where the scattering length exceeds all length scales in the system. Surprisingly, we observe stable sound propagation with low damping for all scattering lengths $|a_{BF}| > 3{,}000\,a_0$ (see Fig. 4) re-

gardless of which side of the resonance the samples are initially prepared on [20]. We label this range the resonant regime. Examples of the sound propagation in the resonant regime are shown in Fig. 4a. An interesting scenario occurs when we approach the resonance from the attractive side. The damping rate increases as the sound velocity approaches zero for stronger attraction until the sound propagation becomes unstable at the critical value $a_c = -790(10)\,a_0$. Then, between a_c and $a_{BF} = -3{,}000\,a_0$ the system does not exhibit stable sound propagation. For even stronger attraction $a_{BF} < -3{,}000\,a_0$, intriguingly, stable sound propagation re-emerges and persists across the Feshbach resonance with a damping and sound velocity comparable to weakly interacting samples. Additional data over this region is presented in the supplement [20].

The stable sound propagation we observe across the interspecies Feshbach resonance goes beyond the mean-field picture and offers promising prospects for future discoveries in the strong-coupling regime. The re-emergence of the sound propagation occurs near the Efimov resonance at the scattering length $a_{BF} = -3{,}330\,a_0$ [28]. Theoretically an Efimov resonance can induce an effective two-body repulsion [38] and stabilize sound propagation. Also, at strong interactions, mean-field corrections are predicted to support a novel quantum droplet phase for scattering lengths $a_{BF} < -750\,a_0$ [39]. Finally, at strong coupling, p-wave fermionic superfluidity is conjectured when fermions are paired through the exchange of bosonic excitations [15, 18, 40], which we estimate would occur in our system in the range $a_{BF} = -2{,}000\,a_0$ to $-10{,}000\,a_0$. The stable phonon propagation we observe near the Feshbach resonance offers promising prospects to explore these intriguing physics with strongly interacting Bose-Fermi mixtures. For example, experimentally probing the interspecies correlations can help elucidate the mechanism that stabilizes the sound mode in the resonant regime.

[1] W. E. Lamb and R. C. Retherford, Phys. Rev. **72**, 241 (1947).

[2] J. Schwinger, Phys. Rev. **73**, 416 (1948).

[3] J. Bardeen, L. N. Cooper, and J. R. Schrieffer, Phys. Rev. **106**, 162 (1957).

[4] G. Giustino, Rev. Mod. Phys. **89** (2017).

[5] B. Keimer, S. A. Kivelson, M. R. Norman, S. Uchida, and J. Zaanen, Nature **518**, 179 (2015).

[6] C. Chin, R. Grimm, P. Julienne, and E. Tiesinga, Rev. Mod. Phys. **82**, 1225 (2010).

[7] K. Günter, T. Stöferle, H. Moritz, M. Köhl, and T. Esslinger, Phys. Rev. Lett. **96**, 180402 (2006).

[8] S. Ospelkaus, C. Ospelkaus, O. Wille, M. Succo, P. Ernst, K. Sengstock, and K. Bongs, Phys. Rev. Lett. **96**, 180403 (2006).

[9] S. Sugawa, K. Inaba, S. Taie, R. Yamazaki, M. Yamashita, and Y. Takahashi, Nature Physics **7**, 642 (2011).

[10] Z. Yan, Y. Ni, C. Robens, and M. W. Zwierlen, Science **368**, 190 (2020).

[11] I. Fritsche, C. Baroni, E. Dobler, E. Kirilov, B. Huang, R. Grimm, G. M. Bruun, and P. Massignan, Phys. Rev. A **103**, 053314 (2021).

[12] M. Delehaye, S. Laurent, I. Ferrier-Barbut, S. Jin, F. Chevy, and C. Salomon, Phys. Rev. Lett. **115**, 265303 (2015).

[13] R. Roy, A. Green, R. Bowler, and S. Gupta, Phys. Rev. Lett. **118**, 055301 (2017).

[14] E. Pazy and A. Vardi, Phys. Rev. A **72**, 033609 (2005).

[15] D. V. Efremov and L. Viverit, Phys. Rev. B **65**, 134519 (2002).

[16] D. Banerjee, M. Dalmonte, M. Müller, E. Rico, P. Stebler, U.-J. Wiese, and P. Zoller, Phys. Rev. Lett. **109**, 175302 (2012).

[17] L. Viverit and S. Giorgini, Phys. Rev. A **66**, 063604 (2002).

[18] T. Enss and W. Zwerger, Eur. Phys. J. B **68**, 383 (2009).

[19] C. Pethick and H. Smith, *Bose-Einstein condensation in dilute gases* (Cambridge University Press, 2002).

[20] See supplementary materials.

[21] M. A. Ruderman and C. Kittel, Phys. Rev. **96**, 99 (1954).

[22] S. De and I. B. Spielman, Applied Physics B **114**, 527 (2014).

[23] B. DeSalvo, K. Patel, G. Cai, and C. Chin, Nature **568**, 61 (2019).

[24] H. Edri, B. Raz, N. Matzliah, N. Davidson, and R. Ozeri, Phys. Rev. Lett. **124**, 163401 (2020).

[25] S. K. Yip, Phys. Rev. A **64**, 023609 (2001).

[26] B. DeSalvo, K. Patel, J. Johansen, and C. Chin, Phys. Rev. Lett. **119**, 233401 (2017).

[27] S. K. Tung, C. Parker, J. Johansen, C. Chin, Y. Wang, and P. S. Julienne, Phys. Rev. A **87** (2013).

[28] J. Johansen, B. J. DeSalvo, K. Patel, and C. Chin, Nat. Phys. **13**, 731 (2017).

[29] M. Berninger, A. Zenesini, B. Huang, W. Harm, H.-C. Nägerl, F. Ferlaino, R. Grimm, P. S. Julienne, and J. M. Hutson, Phys. Rev. A **87**, 032517 (2013).

[30] R. Meppelink, S.B.Koller, and P. van der Straten, Phys. Rev. A **80**, 043605 (2009).

[31] M. R. Andrews, D. M. Kurn, H.-J. Miesner, D. S. Durfee, C. G. Townsend, S. Inouye, and W. Ketterle, Phys. Rev. Lett. **79**, 553 (1997).

[32] J. Joseph, B. Clancy, L. Luo, J. Kinast, A. Turlapov, and J. E. Thomas, Phys. Rev. Lett. **98**, 170401 (2007).

[33] G. Kavoulakis and C. J. Pethick, Phys. Rev. A **58**, 1563 (1998).

[34] K. Mølmer, Phys. Rev. Lett. **80**, 1804 (1998).

[35] L. Viverit, C. J. Pethick, and H. Smith, Phys. Rev. A **61**, 053605 (2000).

[36] R. S. Lous, I. Fritsche, M. Jag, F. Lehmann, E. Kirilov, B. Huang, and R. Grimm, Phys. Rev. Lett. **120**, 243403 (2018).

[37] A. Belemuk, V. Rhyzov, and S.-T. Chui, Phys. Rev. A **76**, 013609 (2007).

[38] T. Enss, B. Tran, M. Rautenberg, M. Gerken, E. Lippi, M. Drescher, B. Zhu, M. Weidemueller, and M. Salmhofer, Phys. Rev. A **102**, 066321 (2020).

[39] D. Rakshit, T. Karpiuk, M. Brewcyzk, and M. Gajda, SciPost Phys. **6**, 079 (2019).

[40] J. Kinnunen, Z. Wu, and G. M. Bruun, Phys. Rev. Lett. **121**, 253402 (2018).